scientific reports

Check for updates

OPEN

Lavender Exosome-Like nanoparticles attenuate UVB-Induced Photoaging via miR166-Mediated inflammation and collagen regulation

Sixu Li[1,5], Fei Liu[2,5], Song Zhang[1,5], Xin Sun[1,5], Xiaojing Li[4], Qiulin Yue[1], Le Su[1,3]✉, Suzhen Yang[2]✉ & Lin Zhao[1]✉

Excessive UVB exposure accelerates skin aging by triggering inflammatory responses and collagen degradation. In recent years, plant-derived extracellular vesicles (PDEVs) have attracted considerable attention for their ability to encapsulate and deliver bioactive molecules, showing therapeutic potential in various fields such as skin care, wound healing, immune regulation, cancer therapy, and drug delivery. In this study, we isolated lavender exosome-like nanoparticles (LELNs) and evaluated their protective effects against UVB-induced skin photoaging. LELNs were purified using differential and sucrose density gradient centrifugation, with characterization through dynamic light scattering (DLS), nanoparticle tracking analysis (NTA), and transmission electron microscopy (TEM). UVB-induced photoaging models were established in HaCaT cells and mice. Treatment with LELNs reduced inflammatory cytokine levels (IL-1β, IL-6, TNF-α) in cell culture supernatants and mouse dorsal skin homogenates. Histopathological staining revealed significant improvements in epidermal thickness, collagen preservation, and overall skin integrity. Through high-throughput small RNA sequencing and transfection of miRNA mimics analysis, we identified key miRNAs in LELNs, particularly cpa-miR166e and zma-miR166h-3p, both of which belonged to the miR166 family and played a critical role in regulating inflammation and collagen metabolism. Functional enrichment analysis indicated that these miRNAs in LELNs were involved in DNA repair, oxidative stress response, and collagen synthesis pathways. Our findings highlight the potential of LELNs as a novel, natural therapeutic strategy for preventing and treating UVB-induced skin photoaging, offering insights into the use of plant-derived extracellular vesicles in dermatological applications.

Keywords Lavender petal, Plant-derived extracellular vesicles, Skin aging, HaCaT, MiRNAs

Cutaneous aging constitutes a natural component of the systemic aging process. It refers to the gradual decline in the structure and function of the skin caused by genetic factors, hormonal changes, and environmental influences[1]. There are two main types of skin aging: intrinsic and extrinsic. Intrinsic aging is driven by natural factors like genetic regulation, slower metabolism, and cellular aging. It often results in dryness, reduced elasticity, and fine lines[2]. Extrinsic aging, on the other hand, is caused by environmental stress, such as UV radiation, air pollution, and unhealthy lifestyle habits. Among these, photoaging, caused by UV exposure, is the most significant type of extrinsic aging[3]. As the body's largest organ, the skin acts as the first line of defense against external threats. It also supports immune protection, temperature regulation, and sensory perception[4]. Aging weakens the skin's barrier function, making it less effective at protecting against pathogens and environmental damage. Understanding how skin aging occurs and finding ways to prevent or slow it down are important. In

[1]State Key Laboratory of Biobased Material and Green Papermaking, School of Bioengineering, Qilu University of Technology, Shandong Academy of Sciences, Jinan 250353, China. [2]Shandong Freda Biotech Co., Ltd, 250101 Jinan, Shandong, China. [3]Shengsheng Xiangrong Biotechnology (Shandong) Co., Ltd, Jinan, P.R. China. [4]Shandong Product Quality Inspection and Research Institute, Jinan, Shandong, China. [5]These authors contributed equally: Sixu Li, Fei Liu, Song Zhang and Xin Sun. ✉email: sule@sdu.edu.cn; 85844202@qq.com; sdilizhaolin@163.com

particular, identifying active compounds that reduce photoaging can play a key role in developing effective treatments and skincare products[5,6].

Ultraviolet radiation (UVR), particularly UVB (280–320 nm), is a major environmental factor in skin aging, leading to photoaging through mechanisms such as DNA damage, reactive oxygen species (ROS) generation, inflammatory responses, and collagen degradation[7]. UVB-induced DNA damage, like cyclobutane pyrimidine dimers (CPDs), can cause mutations and genomic instability, while excessive ROS harms lipids, proteins, and DNA, triggering inflammation and immune suppression[8]. UVB also stimulates the production of matrix metalloproteinases (MMPs), especially MMP-1, which degrade collagen, leading to skin sagging, thinning, and wrinkle formation. Additionally, UVB promotes inflammation by activating dendritic cells and inflammatory cytokines (e.g., IL-6, IL-1β, TNF-α) and causes epidermal thickening due to disrupted cell metabolism. Preventing UVB-induced damage and enhancing repair mechanisms are essential strategies for delaying skin photoaging[9,10].

In recent years, exosome-like nanoparticles (ELNs) have gained considerable attention as key mediators of intercellular communication in both animals and plants[11,12]. These nanoparticles, which range in size from 30 to 200 nm, are secreted by various cell types and carry bioactive molecules such as small RNAs, proteins, lipids, and carbohydrates[13]. They can interact with cells to regulate their functions and play critical roles in a variety of physiological and pathological processes. Plant-derived exosome-like nanoparticles (PELNs), as a novel class of biological carriers, have garnered increasing interest due to their unique biological properties, such as biodegradability, low immunogenicity, and minimal side effects, making them promising candidates for therapeutic applications in medicine and drug delivery[14,15].

ELNs are not only crucial for intercellular communication but also play a significant role in immune regulation, antioxidation, anti-inflammation, and tissue repair. These nanoparticles, which contain bioactive molecules such as small RNAs (miRNAs), can modulate gene expression in recipient cells, thereby influencing cell metabolism, proliferation, differentiation, and migration[16–18]. In recent years, miRNAs derived from ELNs have gained increasing attention in biological research, with their contributions to cellular communication and gene regulation being widely recognized[19,20]. Beyond serving as bridges for intercellular communication, these miRNAs have potential therapeutic applications in aging, inflammation, immune modulation, and cancer metastasis. As research advances, PELNs have shown significant promise, particularly in skin repair, anti-aging, and related therapeutic applications. The miRNAs within these nanoparticles can regulate signaling pathways in recipient cells, influencing various biological processes, such as inflammation, oxidative stress, and tissue repair[21]. Therefore, plant-derived exosome-like nanoparticles hold great potential for therapeutic applications in skin care, anti-aging, and injury repair. Strawberry-derived exosome-like nanoparticles have been shown to effectively prevent oxidative stress in human mesenchymal stromal cells[22]. Wheat-derived nanovesicles have demonstrated significant potential in promoting wound healing[23]. Grapefruit-derived extracellular vesicles exhibit both anti-inflammatory properties and wound-healing acceleration[24]. Tea-derived extracellular vesicles can mitigate inflammatory responses by inhibiting the expression of pro-inflammatory factors[25]. Additionally, carrot-derived nanovesicles show excellent performance in significantly reducing reactive oxygen species (ROS) production and preventing cell apoptosis[26]. As research progresses, these natural nanoparticles may pave the way for new strategies in precision medicine and regenerative therapies.

Lavender (Lavandula angustifolia) has a long history of use in traditional medicine and is widely known for its therapeutic properties. Lavender extracts have been extensively studied for their sedative, anti-inflammatory, antioxidant, and antimicrobial effects, which have been applied in various skincare products and are commonly used for treating skin inflammation and UV-induced skin damage[27]. Many studies have shown that lavender extracts effectively alleviate oxidative stress caused by UV exposure, promote collagen synthesis, and delay skin aging[28,29]. However, despite the extensive research on lavender extracts, studies on lavender exosome-like nanoparticles (LELNs) remain relatively scarce, especially in terms of their application for skin health and anti-aging effects.

This study aims to investigate the anti-photoaging effects of lavender exosome-like nanoparticles (LELNs) against UVB-induced skin damage. Using both in vitro HaCaT cell models and in vivo UVB-irradiated mouse skin models, we first demonstrated the protective roles of LELNs in reducing skin aging and inflammation. The second objective was to identify and characterize the bioactive miRNAs contained within LELNs that mediate these protective effects. Through miRNA sequencing and genomic annotation, key candidate miRNAs were pinpointed that modulate essential biological processes, including DNA repair, anti-inflammatory signaling, antioxidant defense, and collagen synthesis. These findings lay a foundation for understanding the molecular mechanisms underlying the anti-photoaging effects of miRNAs and support their potential therapeutic applications in skin protection.

Materials and methods

Reagents and materials

Dulbecco's Modified Eagle's Medium (DMEM), penicillin-streptomycin solution (SP), and trypsin-EDTA (0.25%) were supplied by Procell Life Sciences Co., Ltd. Fetal bovine serum (FBS) was obtained from ExCell Bio Co., Ltd. Minimum Essential Medium (MEM) was obtained from Gibco (USA). The BCA Protein Assay Kit and RIPA Lysis Buffer were provided by Beyotime Biotechnology Co., Ltd. The transfection reagent Lipofectamine^{TM} 3000 was purchased from Thermo Fisher Scientific (Waltham, MA, USA). ELISA kits for IL-1β, IL-6, IL-8, and TNF-α were sourced from Dakewe Biotech Co., Ltd., while COI-I, MMP-1, and MMP-3 ELISA kits were purchased from Cusabio Biotech (Wuhan, China). Masson's Trichrome Stain Kit, Hematoxylin-Eosin (HE) Stain Kit, DMSO (Dimethyl sulfoxide), and Thiazolyl Blue Tetrazolium Bromide (MTT) were obtained from Solarbio (China). The miRNA extraction kits, reverse transcription kits, SYBR-Green fluorescent dye, and miRNA mimics were purchased from Hunan Aikeri Bioengineering Co., Ltd.

LELNs isolation

Commercially purchased dried lavender flowers of the "Space Blue" variety, sourced from Ili, Xinjiang, were finely ground to a consistency of 3000 mesh and then meticulously mixed with phosphate-buffered saline (PBS) at a volume ratio of 1:10. This homogeneous mixture was subsequently subjected to a low-temperature centrifugation process at 4℃, where it underwent initial centrifugation at 5000 g for 30 min, followed by secondary centrifugation at 10,000 g for 1 h, aimed at effectively removing impurities. The resultant supernatant was then processed through ultracentrifugation (Beckman Optima XPN-100 Ultracentrifuge) at 4℃ and 150,000 g for 1 h, facilitating the precipitation of exosomes, which were ultimately resuspended in 200 μL of PBS. The collected PBS-exosome suspension was subjected to sucrose density gradient centrifugation following established experimental protocols to remove contaminating proteins and other non-exosome vesicles[12].

LELNs identification

Dynamic light scattering (DLS) was employed to measure the particle size and zeta potential of LELNs. Nanoparticle tracking analysis (NTA) was subsequently utilized to validate the vesicle diameter and assess vesicle concentration. A total of 30 μL of the LELNs sample was placed onto a copper grid, and transmission electron microscopy (TEM) was performed at 80 kV for morphological characterization of the nanovesicles.

Cell culture and development of photoaged model

Human immortalized keratinocyte cells (HaCaT cells) were obtained from the Chinese Academy of Sciences Cell Bank and cultured in complete medium (DMEM) containing 10% FBS and 1% SP, maintained in a 37 °C incubator with 5% CO_2. HaCaT cells were cultured in 96-well plates at a density of 10^4 cells per well. After allowing the cells to adhere for 12 h, the original complete medium was discarded and replaced with PBS. Based on previous experiments, 60 mJ/cm² UVB irradiation was determined to be the optimal irradiation intensity[30].

MTT assay and ELISA detection

HaCaT cells were cultured in 96-well plates and, after establishing the photoaging model, treated with different concentrations of LELNs (0.156, 0.312, 0.625, 1.25, 2.5, 5 μg/mL) for 48 h. Add 20 μL of MTT solution to each well and incubate for an additional 4 h. Then, add 100 μL of DMSO to each well, shake for 10 min, and measure the absorbance at 570 nm using a microplate reader. The normal group was not subjected to UVB irradiation and did not receive LELNs treatment; the model group was irradiated with UVB but did not receive LELNs treatment; and the positive control group was treated with Dexamethasone (DEX) after UVB irradiation.

HaCaT cells were cultured in 12-well plates, and subjected to UVB modeling and sample treatment following the same procedure as the MTT assay. After 48 h, the cell culture supernatants were collected for ELISA analysis, including IL-6, IL-8, IL-1β, TNF-α, MMP-1, MMP-3, and Type I Collagen (COI-I).

Animal care and grouping

ICR mice (female, 4–6 weeks old, weighing 18–20 g) were obtained from Beijing Vital River Laboratory Animal Technology Co., Ltd. The mice were acclimatized in an animal facility for one week under controlled conditions (temperature range of 20 to 25 °C, relative humidity of 40–70%, and a 12:12 light/dark cycle) with ad libitum access to food and water. All experimental procedures and animal care were conducted under the national standard "Requirements for the Environment and Housing Facilities of Laboratory Animals" (GB 14925 – 2010) and adhered to the guidelines established by the National Research Council's Guide for the Care and Use of Laboratory Animals. The study was approved by the Animal Ethics Committee of Qilu University of Technology (Shandong Academy of Sciences) (Approval No. SWS20230711).

The mice were randomly assigned to six groups ($n = 7$): (1) N: normal group (no UVB irradiation), (2) M: model group (UVB irradiation only), (3) C: control group (DEX solution + UVB irradiation), (4) L-L: low-dose LELNs group (1 μg/μL LELNs + UVB irradiation), (5) L-M: medium-dose LELNs group (10 μg/μL LELNs + UVB irradiation), and (6) L-H: high-dose LELNs group (100 μg/μL LELNs + UVB irradiation).

UVB irradiation protocol and treatment

Before the initiation of UVB exposure, the dorsal hair of each mouse was carefully removed using an electric shaver, followed by the application of a depilatory cream to ensure a clean, hairless surface for uniform and consistent irradiation. The photoaging model was established by exposing the mice to progressively increasing doses of UVB radiation over a continuous 14-day period. Specifically, an initial dose of 100 mJ/cm² was administered once daily for the first three consecutive days. Subsequently, the irradiation dose was incrementally increased by 50 mJ/cm² every two days, culminating in a final dose of 400 mJ/cm² on day 14.

Before each UVB irradiation session, the assigned topical treatment, including DEX solution or different concentrations of LELNs, was evenly applied to the exposed dorsal skin of the mice. The treatments were applied once daily, immediately before each UVB exposure, and maintained consistently throughout the entire 14-day experimental period.

At the end of the experiment, all mice were terminated, and the dorsal skin tissues were photographed and preserved for subsequent histopathological and biochemical analyses.

Measurement of skin moisture content

The dorsal skin tissue was dried at 105 °C for 4 h until the mass of the sample became constant. The moisture content of the skin was determined using the following equation:

The moisture content of skin (%) = (m1 - m2)/m2 × 100%.

In this formula, m1 indicates the wet weight of the skin, while m2 represents the dry weight[31].

Histological analysis of skin

Skin tissues from the backs of each group of mice were fixed in 4% tissue fixative for 24 h. Following fixation, the tissues were dehydrated using a series of graded alcohols and then immersed in melted paraffin at 65 °C. Once the paraffin blocks solidified, the samples were cut into 4 μm thick sections. The skin morphology was examined using hematoxylin-eosin (HE) staining, while collagen deposition was assessed through Masson's trichrome staining. The stained sections were analyzed with an optical microscope.

Measurement of inflammatory factors and collagen in mouse dorsal skin

The dorsal skin from the mice was homogenized in RIPA buffer (1:9, m/v) and then centrifuged at 3000 rpm for 15 min at 4 °C. The supernatant was collected for analysis. The concentrations of COI-I, MMP-1, MMP-3, IL-1β, IL-6, and TNF-α in the skin were measured using ELISA kits.

Genome annotation and small RNA sequencing analysis

Genome annotation and small RNA sequencing analysis were conducted, including repeat sequence annotation, gene annotation, and non-coding RNA annotation for the LELNs (Completed by Beijing Novogene Technology Co., Ltd.). The total RNA content and fragment distribution of extracellular vesicles were accurately assessed using the Agilent 2100 bioanalyzer with the RNA 6000 Pico Kit. After passing quality control, small RNA libraries were constructed using the Small RNA Sample Pre Kit. The completed libraries were preliminarily quantified using a Qubit 2.0 fluorometer and diluted to 1 ng/μL. Subsequently, the insert size of the libraries was assessed with the high-sensitivity Agilent 2100 system. Once the insert size met expectations, the effective concentration of the libraries (>2 nM) was precisely quantified using qPCR to ensure library quality. Qualified libraries were then subjected to high-throughput sequencing on the Illumina platform using the SE50 strategy.

For miRNA analysis, the miR Evo and miRDeep2 software were used to identify known and predict novel miRNAs. Target genes of the identified miRNAs were predicted using the Target Finder tool. Gene Ontology (GO) annotation was performed using Inter Pro Scan, and Kyoto Encyclopedia of Genes and Genomes (KEGG) pathway annotation was carried out using KOBAS. GO and KEGG enrichment analyses of the predicted target genes were performed with the cluster Profiler package. Enrichment results were considered statistically significant when the adjusted p-value (pad j) was less than 0.05.

the MiRNA transfection and RT-qPCR

RT-qPCR was performed to validate the sequencing results, and based on relative expression levels, four miRNAs, namely cpa-miR166e, zma-miR166h-3p, ath-miR159a, and novel-19, were selected for mimic design and transfection experiments. HaCaT cells were seeded in a 6-well plate, and when the cell density reached 70%, UVB irradiation modeling was performed followed by transfection with miRNA mimics. According to the Lipofectamine 3000 transfection protocol, the mimics and mimics negative control (NC), and inhibitor NC were transfected into the cells. After 72 h of incubation, RT-qPCR was performed to confirm successful transfection. Subsequently, ELISA was conducted on the cell culture supernatants to identify the miRNAs in LELNs that exhibit anti-inflammatory effects and mitigate photoaging.

Statistical analysis

All final data are presented as mean ± standard deviation (SD). All *p*-values were calculated in GraphPad Prism software 9.5 (GraphPad Software Inc., USA). The data were statistically analyzed using the student's t-test. Significance criteria: $^{*}P < 0.05$, $^{**}P < 0.01$.

Result

Isolation and characterization of LELNs

Purified LELNs were obtained using ultracentrifugation and sucrose density gradient centrifugation, and suspended in PBS. Transmission electron microscopy (TEM) images revealed that the extracted LELNs exhibited intact membrane structures and characteristic cup-shaped vesicles (Fig. 1A). Nanoparticle tracking analysis (NTA) showed that the exosome concentration was 3.75×10^{11} particles/mL (Fig. 1B). Dynamic light scattering (DLS) analysis indicated that the average vesicle diameter of the LELNs was 160.1 nm (Fig. 1C), which was consistent with the TEM and NTA results. Additionally, the zeta potential was measured at −26.6 mV (Fig. 1D), which is indicative of the typical negative charge associated with exosomes.

Protective effects of LELNs on UVB-Induced Photoaging and inflammatory response in HaCaT cells

Prior to the cell viability assays, we performed preliminary experiments to determine the UVB irradiation intensity required to establish the HaCaT cell photoaging model. Following this, we conducted an MTT assay to assess the effect of different concentrations of LELNs (0.156, 0.312, 0.625, 1.25, 2.5, and 5 μg/mL) on the viability of UVB-induced photoaging HaCaT cells. The results as shown in Fig. 2A, indicated that UVB irradiation reduced the cell viability of HaCaT cells to 45.9%. However, after treatment with various concentrations of LELNs, cell viability increased by 21.86%, 19.46%, 12.09%, 9.97%, 14.5%, and 8.04%, respectively, compared to the model group, showing a significant improvement in cell survival. Notably, at the low concentrations of 0.156 and 0.312 μg/mL, there was no significant difference in cell viability compared with the positive control group.

Next, we used ELISA kits to measure the levels of inflammatory cytokines, COI-I, and matrix metalloproteinases (MMPs) in the cell culture supernatants. As illustrated in Fig. 2, the results revealed a significant increase in the levels of these inflammatory factors and MMPs following UVB irradiation. However, treatment with different concentrations of LELNs significantly reduced the levels of these factors, bringing them closer to the levels observed in the normal group. In Fig. 2E, the TNF-α levels in the 0.156 and 0.312 μg/mL LELNs-treated groups

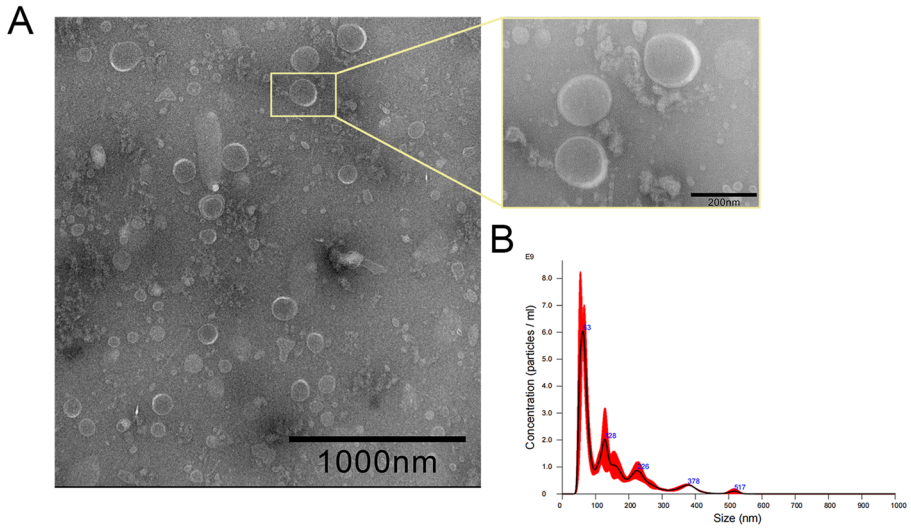

C

		Size (d.nm):	% Volume:	St Dev (d.nm):	
Z-Average (d.nm): 181.1	Peak 1:	160.1	100.0	42.31	D(10.nm): 124
PdI: 0.106	Peak 2:	0.000	0.0	0.000	D(50.nm): 168
Intercept: 0.966	Peak 3:	0.000	0.0	0.000	D(90.nm): 232

Result quality : Refer to quality report

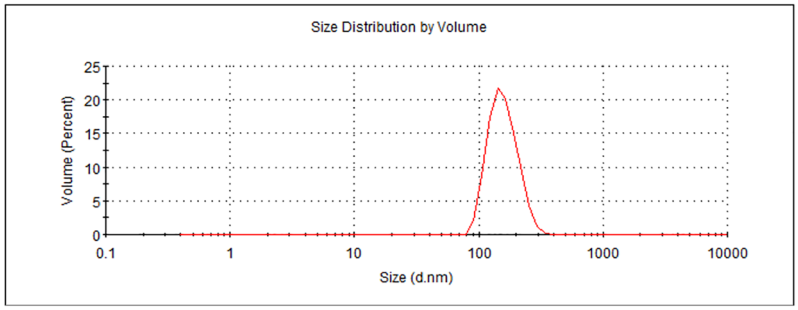

D

		Mean (mV)	Area (%)	St Dev (mV)
Zeta Potential (mV): -26.1	Peak 1:	-26.6	100.0	6.82
Zeta Deviation (mV): 5.90	Peak 2:	0.00	0.0	0.00
Conductivity (mS/cm): 1.34	Peak 3:	0.00	0.0	0.00

Result quality : Good

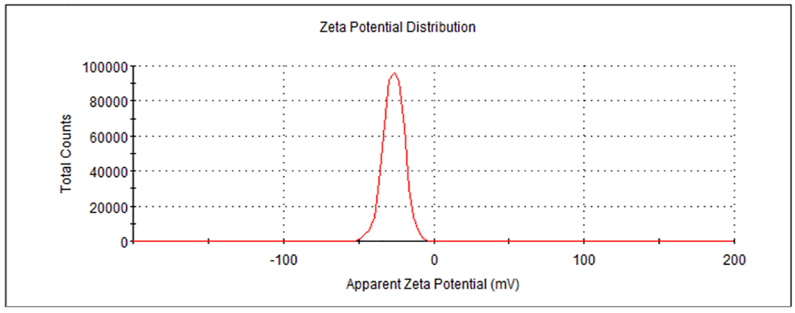

Fig. 1. Extraction and characterization of LELNs. LELNs were isolated and purified using high-speed centrifugation and sucrose density gradient centrifugation. (**A**) Transmission electron microscopy (TEM) image of LELNs. Vesicle enrichment is observed and magnified views show vesicles with an approximate diameter of 160 nm (scale bar: 200 nm). (**B**) Size distribution and concentration of LELNs were analyzed by nanoparticle tracking analysis (NTA). The y-axis represents the vesicle particle concentration, and the x-axis represents the vesicle diameter. (**C**) Particle size analysis of LELNs. (D) Zeta potential analysis of LELNs.

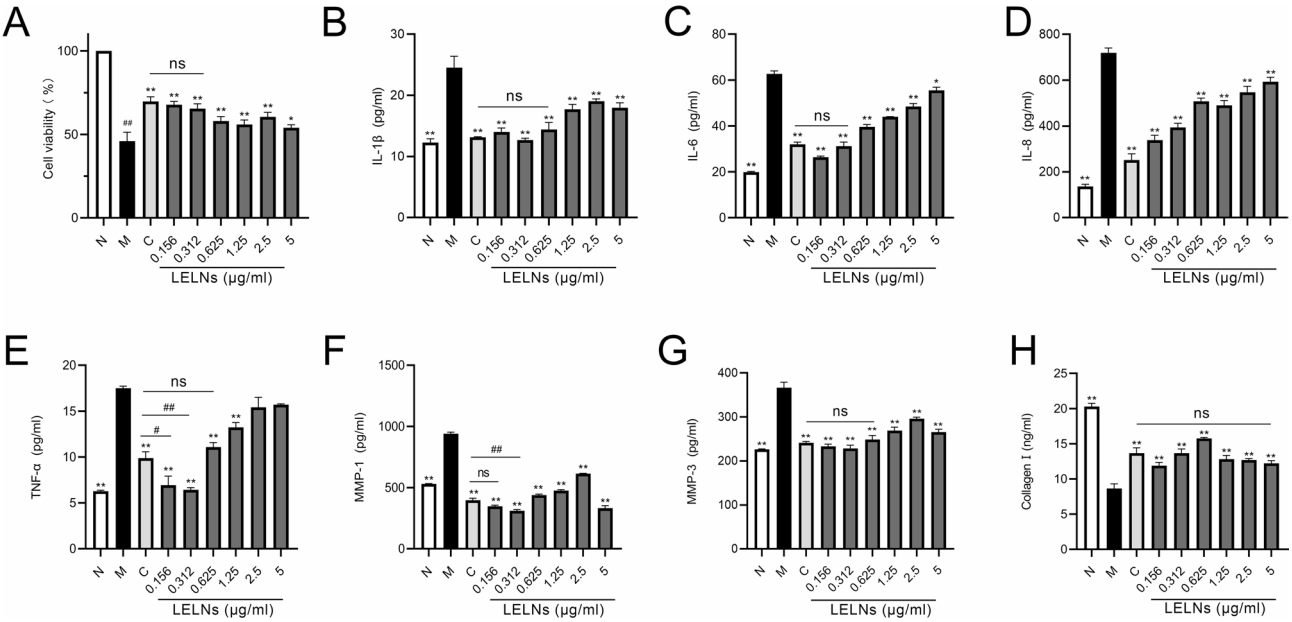

Fig. 2. Protective effects of LELNs on UVB-induced photoaging in HaCaT cells. (**A**) Effect of LELNs on the viability of UVB-induced photoaged HaCaT cells (##$P<0.01$ vs. N, *$P<0.05$, **$P<0.01$ vs. M, ns vs. C). (B-H) Effects of LELNs on the expression levels of inflammatory cytokines and extracellular matrix-related markers in UVB-induced photoaged HaCaT cells: IL-1β (**B**), IL-6 (**C**), IL-8 (**D**), TNF-α (**E**), MMP-1 (**F**), MMP-3 (**G**), and COI- I (**H**) (*$P<0.05$, **$P<0.01$ vs. M, #$P<0.05$, ##$P<0.01$ vs. C, $n=3$). N: normal group; M: model group; C: positive control group; 0.156, 0.312, 0.625, 1.25, 2.5, 5 μg/mL: LELNs treatment groups.

were significantly better than those in the positive control (DEX) group. Lastly, we further validated the effects of LELNs by measuring the content of COI-I. Different concentrations of LELNs significantly increased collagen content, with respective increases of 27.26%, 36.67%, 45.07%, 32.50%, 31.83%, and 29.19%. The significance analysis revealed that the effects of LELNs at all concentrations were not significantly different from those of DEX, indicating comparable effectiveness, as shown in Fig. 2H.

Induction of UVB-induced photodamage model in mouse dorsal skin

A large amount of LELNs was extracted using the method shown in Fig. 3A, and a UVB-induced photoaging mouse model was established, with the specific irradiation dose and key experimental time points illustrated in Fig. 3B. After two weeks of UVB irradiation, the dorsal skin of the model group mice exhibited typical signs of photoaging, including roughened and thickened skin, pronounced erythema, widespread desquamation, and deep, visible wrinkles (Fig. 3C). These changes are consistent with the characteristics of photoaging induced by ultraviolet radiation, indicating that UVB exposure caused significant damage to the mouse skin.

In contrast to the model group, the skin of the LELNs-treated mice remained relatively smooth, with only mild desquamation. Overall, the skin condition in the LELNs groups showed considerable improvement. There were no obvious erythema or deep wrinkles in the LELNs-treated groups, suggesting that LELNs had a protective effect in alleviating or repairing UVB-induced photoaging. In the low-concentration group, the wrinkles on the dorsal skin of mice were the shallowest, but slight flaking was observed; in the medium- and high-concentration groups, mild wrinkle patterns were present. These results suggested that LELNs could mitigate UVB-induced skin damage by improving the skin's structure and function, thereby partially slowing down the photoaging process.

Finally, measurement of the total skin hydration in the backs of mice revealed that UVB irradiation caused a significant decrease in skin moisture content, which is closely related to the damage to the skin barrier function and inflammatory responses. However, after LELNs treatment, skin hydration levels increased across all concentration groups, and significance analysis showed no significant differences between any of the LELNs groups and the DEX (Fig. 3D).

Effects of LELNs on UVB-Induced inflammation in mouse dorsal skin

The effect of UV-induced skin damage on the epidermis and dermis of mice is an important approach to studying skin aging and inflammation. Changes in epidermal thickness are one of the key indicators used to evaluate photoaging and inflammatory responses in the skin. In this study, we utilized hematoxylin and eosin (HE) staining to assess the condition of the dorsal skin of mice following UVB irradiation. The results showed that UVB irradiation led to a significant increase in epidermal thickness, accompanied by extensive infiltration of inflammatory cells, as well as disorganized hair follicle arrangement (Fig. 4A). These structural changes were consistent with the macroscopic symptoms of skin barrier damage, indicating that UVB irradiation not only caused epidermal thickening but also exacerbated the inflammatory response in the skin. To further quantify

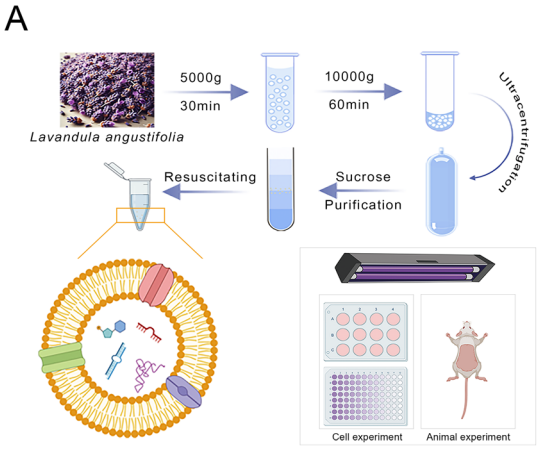

B

Day	UVB Dose (mJ/cm²)	Remarks
Day 1–3	100	1.Daily application to dorsal skin 2.UVB dose increased by 50 mJ/cm²
Day 4–5	150	
Day 6–7	200	
Day 8–9	250	
Day 10–11	300	
Day 12–13	350	
Day 14	400	Final irradiation; skin photographed & collected

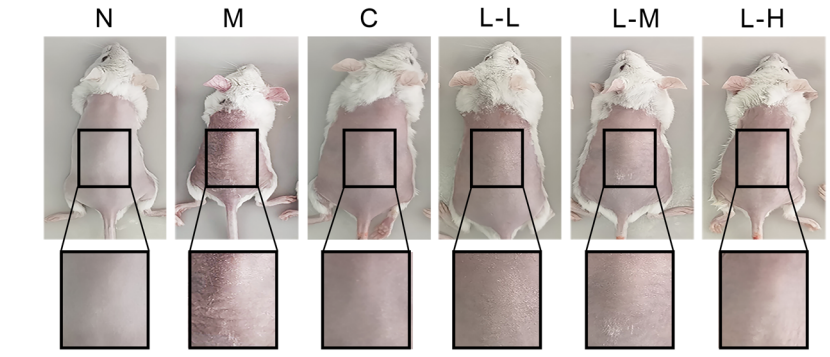

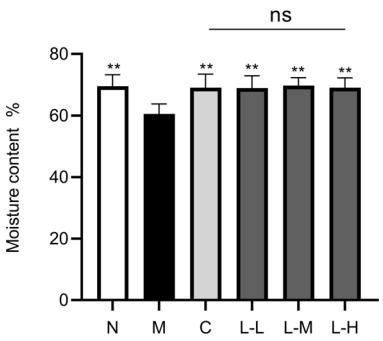

Fig. 3. LELNs extraction and their effects on UVB-induced photoaging in mouse dorsal skin. (**A**) LELNs extraction and photoaging model establishment (**B**) UVB irradiation dosage and key points of photoaging model. (**C**) Dorsal skin condition of mice after UVB-induced photoaging and treatment with LELNs. (**D**) Analysis of skin hydration levels in mouse dorsal skin after drying. (**$P < 0.01$ vs. M, ns vs. C, $n = 7$) N: normal group; M: model group; C: positive control group; L-L: low-dose LELNs group; L-M: medium-dose LELNs group; L-H: high-dose LELNs group.

these histological changes, we measured the epidermal thickness in each group based on HE staining sections. As shown in Fig. 4B, the L-L group significantly reduced the abnormal epidermal thickening induced by UVB irradiation, demonstrating a clear protective effect.

However, after treatment with LELNs, the epidermal thickness of the dorsal skin in mice significantly decreased, suggesting that LELNs may regulate the skin's repair mechanisms and reduce the excessive thickening induced by UVB. Additionally, inflammatory symptoms were notably alleviated, with a reduction in inflammatory cell infiltration, and the hair follicle arrangement returned to a more normal state. These findings suggest that LELNs may effectively mitigate UV-induced skin damage through anti-inflammatory and antioxidant mechanisms, facilitating the repair of damaged skin structures and improving overall skin health.

We assessed the expression levels of several key inflammatory cytokines by ELISA to comprehensively evaluate the anti-inflammatory effect of LELNs. The results showed that UVB irradiation significantly upregulated the levels of inflammatory cytokines IL-1β, IL-6, and TNF-α (Fig. 4C-E). However, after applying LELNs to the dorsal skin of mice, the levels of these inflammatory cytokines were significantly reduced to varying extents, which was consistent with the findings from the HE staining analysis.

Effect of LELNs on collagen changes in UVB-Damaged mouse dorsal skin

Collagen is the main structural component of the dermis and plays a crucial role in maintaining the skin's elasticity and firmness. We used Masson's trichrome staining to investigate the impact of UVB irradiation on collagen in skin tissue (Fig. 5A). The experimental results showed that in the model group subjected to UVB irradiation, collagen fibers in the dermis were significantly reduced, with a noticeable decrease in the blue staining area. The collagen fibers appeared sparse and disorganized, and the spatial density of collagen was markedly reduced. These changes indicate that UVB irradiation led to collagen loss and fiber fragmentation, which negatively affected the structure and function of the skin.

After LELNs treatment, the collagen degradation induced by UVB irradiation was effectively alleviated. In the LELNs-treated group, collagen fibers in the dermis regained a more dense and organized arrangement, with a significant increase in the blue-stained area, indicating that collagen loss and fiber fragmentation were effectively repaired. These results suggest that LELNs have a protective effect and can effectively reduce collagen

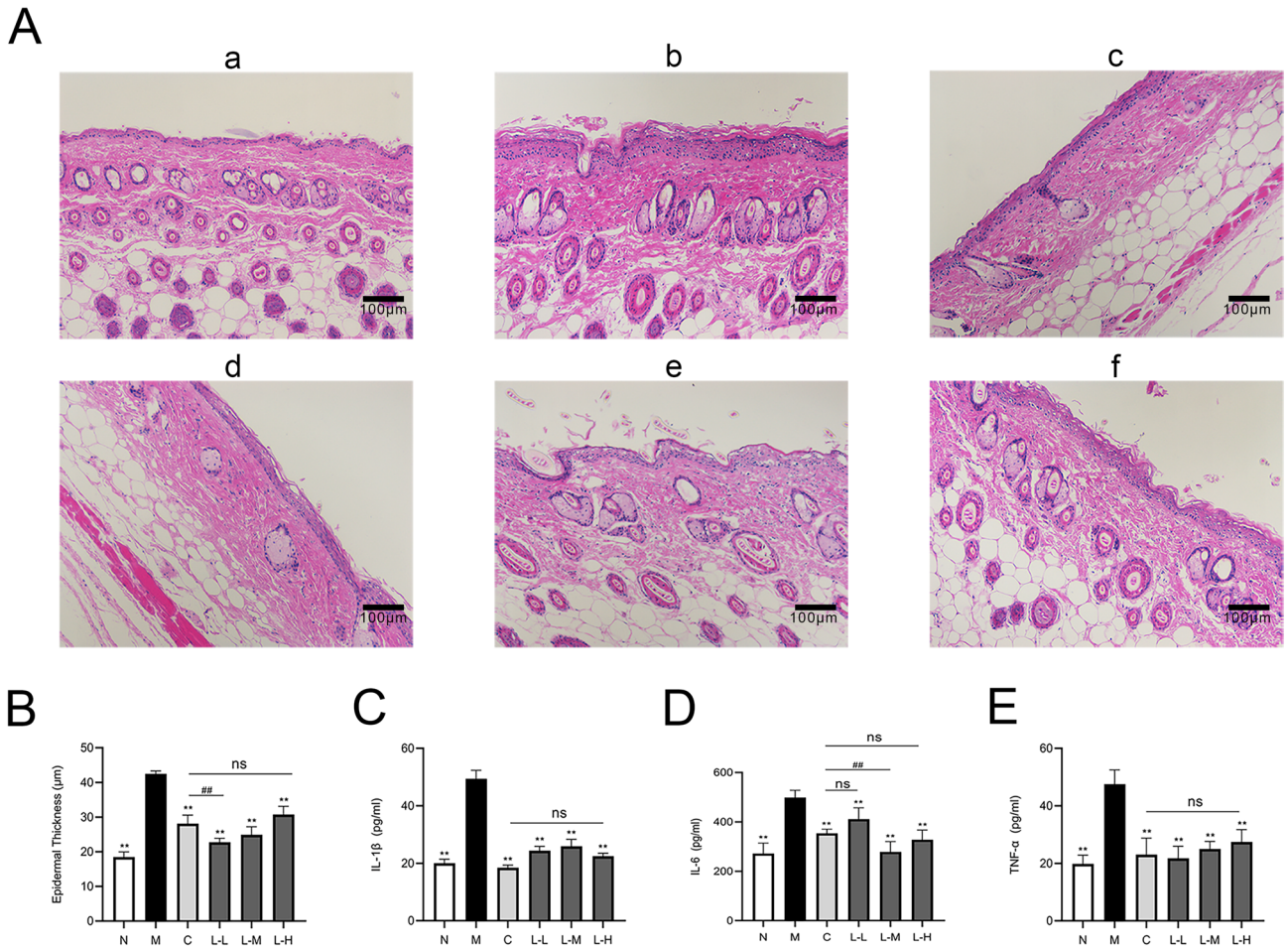

Fig. 4. Histological analysis of mouse dorsal skin and inflammatory cytokine levels. (**A**) Hematoxylin and eosin (HE) staining of mouse dorsal skin tissues ($n = 7$, scale bar = 100 μm). a: normal group; b: model group; c: positive control group; d: low-dose LELNs group; e: medium-dose LELNs group; f: high-dose LELNs group. (**B**) Epidermal thickness measurement (**$P < 0.01$ vs. M, ##$P < 0.01$ vs. C, $n = 7$). (**C**-**E**) Levels of inflammatory cytokines in dorsal skin homogenates: IL-1β (**C**), IL-6 (**D**), and TNF-α (**E**). (**$P < 0.01$ vs. M, ##$P < 0.01$ vs. C, $n = 7$).

degradation caused by UVB irradiation, helping to restore the structural integrity of the skin. To further quantify these changes, we analyzed the collagen fiber area ratio based on Masson-stained sections (Fig. 5B). The results showed that the L-L group notably restored collagen content, with values approaching those of the normal group and showing superior effects compared to the DEX group.

We then measured the levels of COI-I in skin homogenates using ELISA. Since MMPs are key enzymes involved in collagen degradation, we also assessed the levels of MMP-1 and MMP-3. The results showed that, compared to the normal group, the model group exhibited significantly elevated levels of MMPs and reduced levels of COI-I (Fig. 5C-E). However, LELNs treatment was able to reverse this trend, restoring the balance between collagen production and degradation.

Small RNA sequencing analysis of LELNs

We extracted the total small RNAs from LELNs and analyzed their fragment lengths. The results showed that the majority of the small RNA fragments were concentrated in the 18–30 nt range, as shown in Fig. 6A. Through sRNA-seq analysis, we annotated a total of 119 miRNAs, including 70 known miRNAs and 49 novel miRNAs. Based on the ranking of miRNA read counts from the sequencing results, eight known miRNAs (Fig. 6B) with high read counts and four novel miRNAs (Fig. 6C) were selected for qPCR validation, and their miRNA sequences were shown in Fig. 6D. After performing three parallel experiments and normalizing the data, the results showed that four miRNAs, cpa-miR166e, zma-miR166h-3p, ath-miR159a, and novel-19, exhibited significant and stable expression in LELNs (Fig. 6E). Based on these stable and reliable results, these four miRNAs were selected for subsequent transfection experiments.

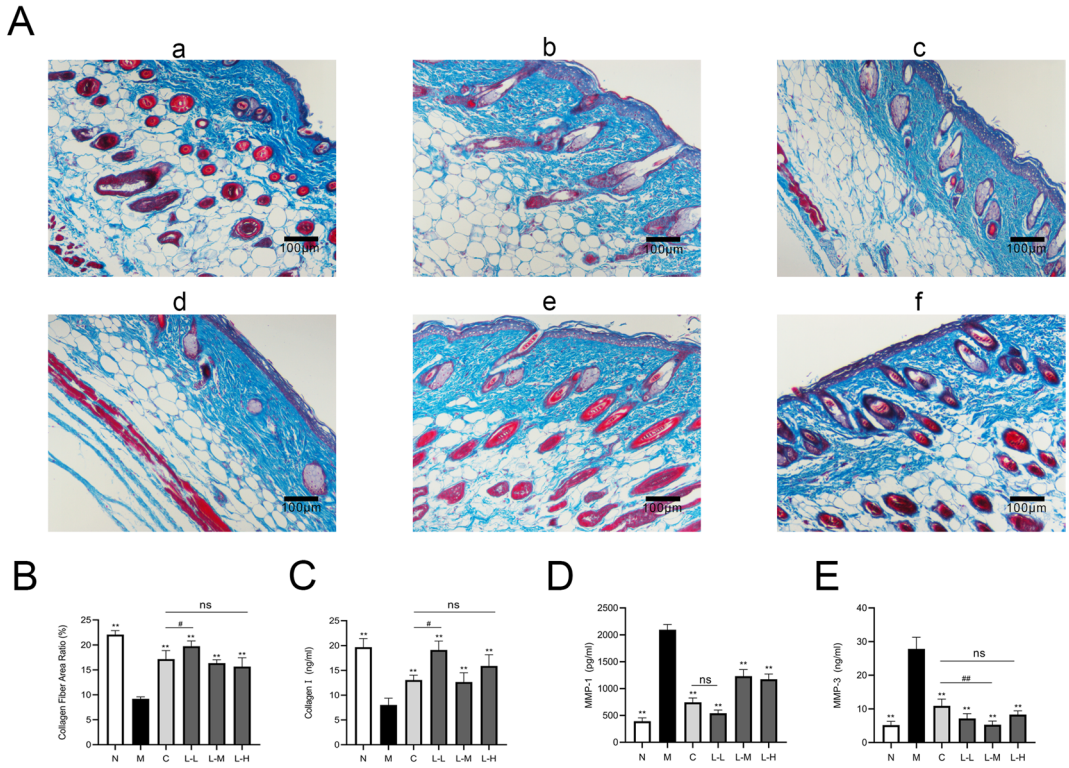

Fig. 5. Histological analysis of collagen deposition and MMP levels in mouse dorsal skin. (**A**) Masson staining of mouse dorsal skin tissues, showing collagen distribution ($n = 7$, scale bar = 100 μm). a: normal group; b: model group; c: positive control group; d: low-dose LELNs group; e: medium-dose LELNs group; f: high-dose LELNs group. (**B**) Quantization of collagen fiber area ratio (**$P < 0.01$ vs. M, #$P < 0.05$ vs. C, $n = 7$). (**C**-**E**) Levels of COI-I (**C**), MMP-1 (**D**), and MMP-3 (**E**) in dorsal skin homogenates. (**$P < 0.01$ vs. M, #$P < 0.05$, ##$P < 0.01$ vs. C, $n = 7$).

The effect of MiRNAs in LELNs on UVB-Induced HaCaT cell damage

To validate the skin repair effects of the four miRNAs mentioned above, we transfected HaCaT cells with four miRNA mimics, inhibitors, mimics NC, and inhibitor NC after UVB irradiation modeling. Cell culture supernatants were collected 72 h post-transfection. RT-qPCR was first performed to assess transfection efficiency, and the CT value results confirmed successful transfection (Fig. 7A). Subsequently, ELISA was conducted on the collected supernatants.

The results showed in Fig. 7, suggested that after UVB irradiation, levels of IL-1β, IL-6, IL-8, TNF-α, MMP-1, and MMP-3 were significantly elevated in the NC group, while COI-I levels markedly decreased. Among the tested miRNAs, ath-miR159a exhibited a pronounced pro-inflammatory effect. In contrast, cpa-miR166e effectively suppressed the elevation of inflammatory cytokines, while cpa-miR166e and zma-miR166h-3p jointly inhibited the increase in matrix metalloproteinases and collagen degradation. Notably, novel-19 did not show any significant effect.

Target gene prediction and gene function analysis

To further explore the mechanisms by which cpa-miR166e and zma-miR166h-3p protect HaCaT cells from UVB-induced damage, we conducted functional enrichment analysis for these two miRNAs (Fig. 8A and B). The results of the Gene Ontology (GO) enrichment analysis revealed that nuclear-related processes (nucleus) and DNA repair exhibited the highest enrichment significance, indicating that the input genes play a critical role in regulating nuclear functions and DNA damage repair. These processes are essential for maintaining genomic stability in skin cells and delaying cellular aging. Additionally, the analysis showed significant enrichment in protein metabolic processes, suggesting that these genes may be involved in collagen synthesis and degradation, contributing to the maintenance of skin structure and functional integrity.

Notably, oxidoreductase activity and mitochondrial-related functions (mitochondrion) also showed a certain degree of enrichment, which is closely associated with oxidative stress and cellular energy metabolism. Oxidative stress is a major factor in skin aging while maintaining mitochondrial function helps reduce reactive oxygen species (ROS) production and delay cellular aging.

The KEGG enrichment analysis revealed that the Glutathione metabolism and Cysteine and methionine metabolism pathways were significantly enriched. These pathways are closely related to oxidative stress, as they regulate the synthesis of glutathione and maintain redox balance, which helps eliminate free radicals, reduce oxidative stress-induced damage to skin cells, inhibit MMP activation, and minimize collagen degradation,

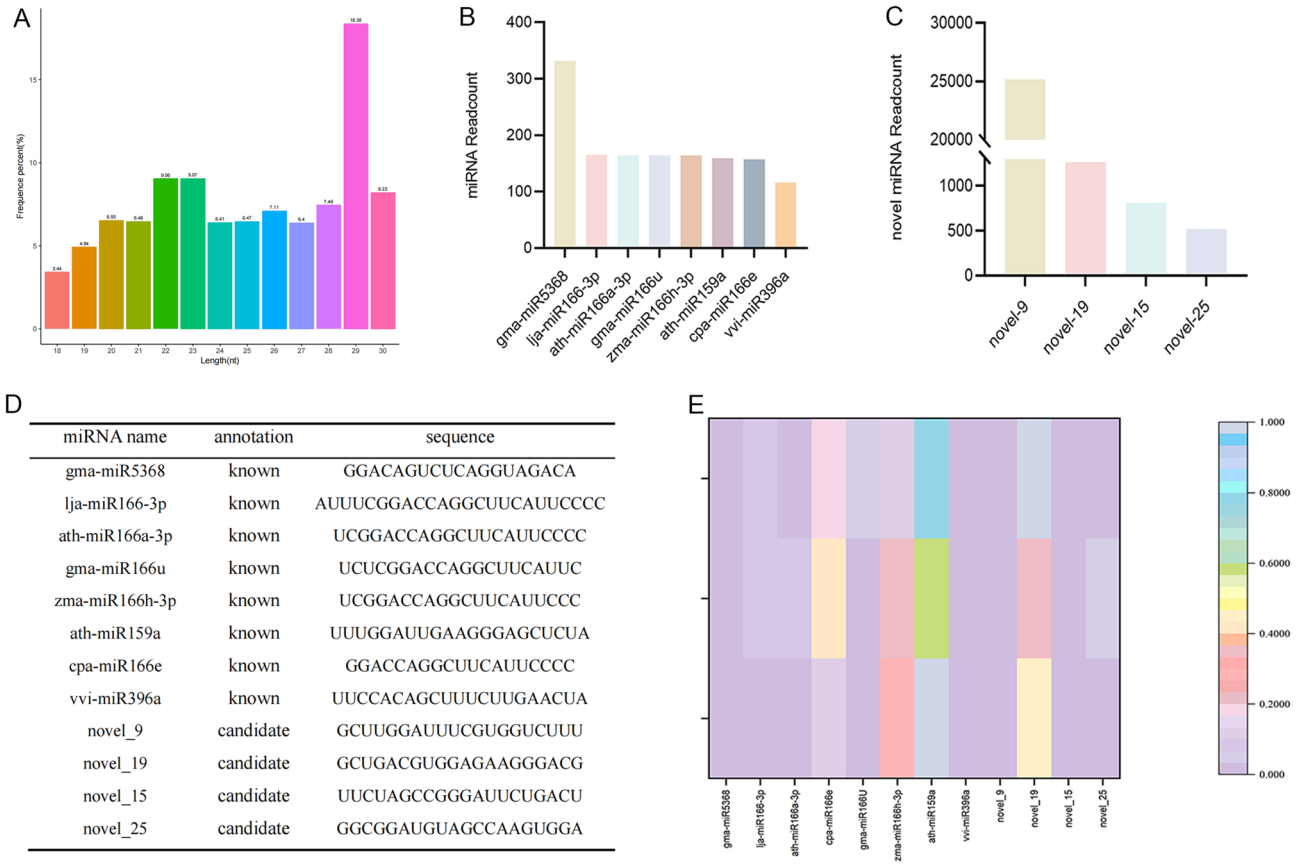

D

miRNA name	annotation	sequence
gma-miR5368	known	GGACAGUCUCAGGUAGACA
lja-miR166-3p	known	AUUUCGGACCAGGCUUCAUUCCCC
ath-miR166a-3p	known	UCGGACCAGGCUUCAUUCCCC
gma-miR166u	known	UCUCGGACCAGGCUUCAUUC
zma-miR166h-3p	known	UCGGACCAGGCUUCAUUCCC
ath-miR159a	known	UUUGGAUUGAAGGGAGCUCUA
cpa-miR166e	known	GGACCAGGCUUCAUUCCCC
vvi-miR396a	known	UUCCACAGCUUUCUUGAACUA
novel_9	candidate	GCUUGGAUUUCGUGGUCUUU
novel_19	candidate	GCUGACGUGGAGAAGGGACG
novel_15	candidate	UUCUAGCCGGGAUUCUGACU
novel_25	candidate	GGCGGAUGUAGCCAAGUGGA

Fig. 6. Identification and validation of miRNAs in LELNs by small RNA high-throughput sequencing. (**A**) Length distribution of miRNAs in LELNs, ranging from 18 to 30 nucleotides. (**B**) Top eight miRNAs with the highest read counts, ranked in descending order. (**C**) Top four predicted novel miRNAs with the highest read counts. (**D**) Sequences of the 12 miRNAs identified through sequencing. (**E**) Validation of the read count results for 12 selected miRNAs using RT-qPCR ($n = 3$).

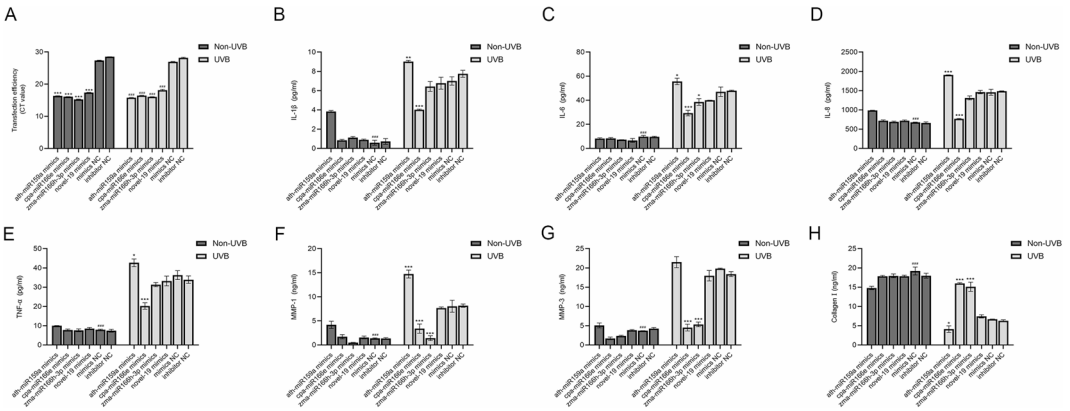

Fig. 7. Effects of miRNA mimics transfection on UVB-induced photoaging in HaCaT cells. (**A**) Analysis of transfection efficiency. (***$P < 0.001$ vs. mimics NC group in the Non-UVB group, ###$P < 0.001$ vs. mimics NC group in the UVB group). (B-H) Effects of transfection with different miRNA mimics on inflammatory cytokines and ECM-related markers in UVB-induced photoaged HaCaT cells: IL-1β (**B**), IL-6 (**C**), IL-8 (**D**), TNF-α (**E**), MMP-1 (**F**), MMP-3 (**G**), and COI- I (**H**). (###$P < 0.001$, *$P < 0.05$, ***$P < 0.001$ vs. mimics NC group in the UVB group, $n = 3$).

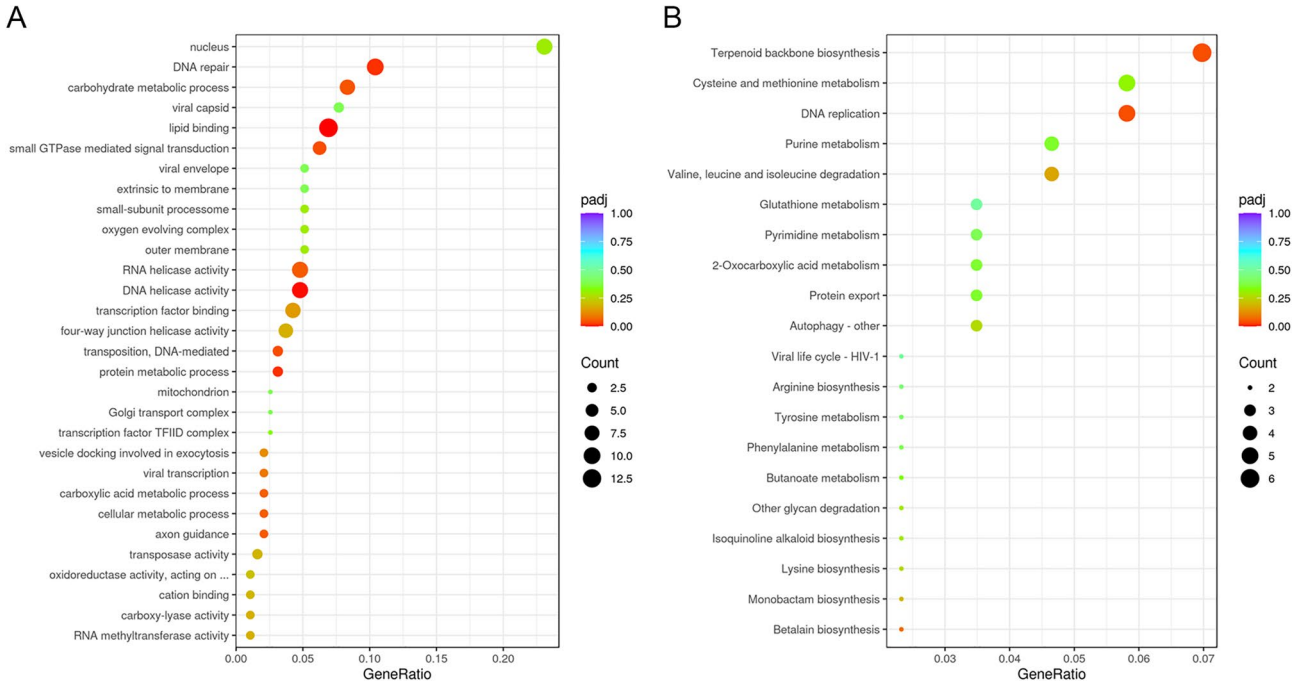

Fig. 8. Functional enrichment analysis of miRNAs identified in LELNs. (**A**) Gene Ontology (GO) enrichment analysis of target genes regulated by miRNAs in LELNs. The y-axis represents significantly enriched GO terms, including "nucleus," "DNA repair," and "carbohydrate metabolic process," among others, with the x-axis indicating the GeneRatio. The size of the dots corresponds to the number of genes, while the color indicates the adjusted p-value (padj). (**B**) Kyoto Encyclopedia of Genes and Genomes (KEGG) pathway enrichment analysis of target genes regulated by miRNAs in LELNs. The y-axis shows significantly enriched pathways, such as "terpenoid backbone biosynthesis," "cysteine and methionine metabolism," and "DNA replication," with the x-axis indicating the GeneRatio. Dot size represents the number of genes enriched in the pathway, and color denotes the adjusted p-value (padj).

thereby delaying skin aging. Additionally, the enrichment of the Protein export pathway suggests that the input genes may play an important role in the synthesis, modification, and secretion of collagen, further maintaining the structural integrity and elasticity of the skin. The enrichment of the DNA replication pathway is also notable, as DNA replication serves as the foundation for cell proliferation and renewal, contributing to the continuous regeneration of basal layer skin cells and ensuring genomic stability, which prevents DNA damage-induced cellular aging or dysfunction. Furthermore, the enrichment of the Autophagy pathway indicates its potential role in clearing damaged proteins and organelles within cells, maintaining intracellular homeostasis, and reducing the accumulation of aging cells.

Discussion

Plant-Derived Extracellular Vesicles as Innovative Therapeutics.

In recent years, scientific research has revealed the significant therapeutic potential of plant-derived extracellular vesicles (EVs) in various biological processes, including antioxidant activity, anti-inflammation, anti-tumor effects, tissue regeneration, and metabolic regulation[32]. As natural nanoscale carriers, plant-derived EVs are enriched with bioactive components such as proteins, lipids, secondary metabolites, and microRNAs (miRNAs), enabling the precise delivery of functional molecules to target cells and the regulation of multiple cellular signaling pathways, thereby exerting multifaceted biological effects[33].

Studies have shown that grape-derived EVs exhibit remarkable effects in inhibiting reactive oxygen species (ROS) production and enhancing cellular antioxidant defense mechanisms while regulating cell cycle pathways to suppress tumor cell proliferation[34]. Ginger-derived EVs can modulate the expression of immune-related genes, enhance macrophage activity, and accelerate the repair of intestinal inflammation[35]. Aloe vera-derived EVs promote extracellular matrix (ECM) remodeling and epithelial cell proliferation, demonstrating their ability to accelerate wound healing and tissue regeneration[36]. These findings further highlight the potential applications of plant-derived EVs in disease repair and health promotion.

EVs and their miRNAs have been shown to exert effects in mammals and across species. As natural nanocarriers, plant EVs interact with host cells to deliver bioactive components, such as proteins, lipids, and miRNAs, to target cells, thereby regulating various biological processes[37,38]. In immune modulation, plant EVs can regulate macrophage function, promote anti-inflammatory responses, and enhance the host's immune response or reduce excessive immune reactions[39,40]. Additionally, the miRNAs and other bioactive components carried by plant EVs have antioxidant and anti-inflammatory effects, modulating oxidative stress

and inflammatory responses in host cells, and alleviating damage caused by environmental stress or diseases[41,42]. Plant EVs also promote tissue repair by supporting cell proliferation and migration, playing roles in wound healing, bone regeneration, and cardiovascular disease repair[43]. Plant miRNAs, such as miR156 and miR166, enter mammalian cells via EVs and regulate gene expression, influencing cellular functions and biological processes, including the cell cycle, DNA repair, and anti-tumor processes[44,45]. Furthermore, the miRNAs in plant EVs can regulate the host's metabolic processes, such as fat and glucose metabolism, offering potential therapeutic value in treating metabolic diseases like obesity and diabetes.

With their natural origin, strong biocompatibility, and ability to deliver functional molecules in a targeted manner, plant-derived EVs can regulate multiple cellular pathways, offering broad application prospects in the fields of antioxidant activity, anti-inflammation, and tissue regeneration. These advantages provide new research directions for developing safe and effective natural therapies.

Unique Characteristics of Lavender-Derived Extracellular Vesicles.

Lavender (Lavandula angustifolia) is widely recognized for its anti-inflammatory and antioxidant properties, primarily attributed to its essential oils and polyphenols[46]. However, this study revealed the unique potential of LELNs in combating UVB-induced skin photoaging. LELNs provide distinct advantages through the delivery of bioactive miRNAs that regulate cellular processes critical to skin regeneration and repair. These miRNAs were shown to influence pathways such as DNA repair and replication, as well as glutathione metabolism, mitigating oxidative stress damage in skin cells. Moreover, LELNs effectively inhibit MMP activity, restoring collagen levels and maintaining ECM structure and function. Compared to other plant-derived EVs, such as those derived from grapes or aloe vera, LELNs demonstrate a more diverse range of effects, regulating multiple pathways simultaneously, including inflammation, ECM remodeling, and oxidative stress response.

Selection and Functional Roles of miRNAs.

One of the key findings of this study is the enrichment of specific miRNAs, such as cpa-miR166e and zma-miR166h-3p, within LELNs. As important post-transcriptional regulators, miRNAs play critical roles in mitigating UVB-induced skin photoaging through multiple pathways. Both cpa-miR166e and zma-miR166h-3p belong to the miR166 family, which is highly conserved in plants. Previous studies have shown that these miRNAs primarily regulate the development of leaf polarity, vascular tissue formation, and root morphology in maize by targeting HD-ZIP III transcription factors[44,47]. Additionally, they are crucial in plant responses to abiotic stresses, such as drought and salt stress, by enhancing the plant's stress tolerance through the regulation of relevant genes. While their roles in plants are well-established, their functions in other species, such as mammals, remain unexplored. In the context of skin photoaging, one of the central mechanisms for counteracting UVB-induced aging is DNA damage repair. UVB radiation generates cyclobutane pyrimidine dimers (CPDs) and other DNA lesions, which, if left unrepaired, can lead to gene mutations, cellular dysfunction, and accelerated aging[48]. The protective role of miRNAs in DNA repair has been well-documented. For instance, miRNAs such as miR-155 and miR-34a are known to regulate key players in the DNA damage response[49,50]. Our findings suggested that cpa-miR166e and zma-miR166h-3p might similarly regulate DNA repair and replication pathways in skin cells, contributing to genomic stability and reducing the accumulation of UVB-induced DNA damage.

In addition to DNA repair, these miRNAs likely influence other critical pathways related to skin anti-aging. For instance, they may modulate oxidative stress response mechanisms, such as the Nrf2/KEAP1 axis, enhancing antioxidant capacity and reducing ROS-induced damage to lipids, proteins, and DNA[51,52]. Furthermore, they may regulate inflammation pathways, suppressing the expression of pro-inflammatory cytokines such as IL-6, IL-1β, and TNF-α, thereby alleviating UVB-induced inflammation[53]. Additionally, the GO enrichment analysis indicated that these miRNAs are involved in protein metabolism and ECM remodeling, which could promote collagen synthesis and deposition, improving skin structure and elasticity. This multifunctional role highlights the ability of LELNs to address various aspects of skin photoaging simultaneously.

Regulation of ECM Integrity and Collagen Synthesis.

UVB-induced photoaging is characterized by collagen degradation and ECM disruption, primarily driven by the upregulation of matrix metalloproteinases (MMPs), such as MMP-1 and MMP-3[54,55]. This study revealed that LELNs effectively inhibited MMP activity, restoring collagen levels and enhancing ECM integrity. Histological analysis confirmed that LELNs not only prevent collagen degradation but also promote collagen fiber synthesis and deposition through protein metabolism-related pathways. This dual function in protecting and repairing ECM structure further supports the potential of LELNs to improve skin elasticity and reduce wrinkles.

Anti-Inflammatory Effects and UVB Damage Mitigation.

UVB-induced inflammation is a major driver of skin photoaging, as UVB radiation activates pro-inflammatory pathways, leading to increased secretion of cytokines such as IL-6, IL-1β, and TNF-α[56]. These cytokines contribute to local inflammation, immune dysregulation, and accelerated aging. This study demonstrated that LELNs significantly downregulate the expression of these cytokines, reduce inflammatory cell infiltration, and alleviate epidermal thickening caused by UVB exposure. This anti-inflammatory effect is likely mediated by miRNA regulation of inflammatory signaling pathways, further supporting the potential of LELNs as an effective treatment for UVB-induced damage.

Conclusion and future directions

In conclusion, LELNs mitigate UVB-induced skin photoaging through multiple mechanisms, including reducing inflammation, enhancing ECM integrity, promoting DNA repair, and mitigating oxidative stress. Among their active components, cpa-miR166e and zma-miR166h-3p are likely mediated by miRNAs that regulate key pathways such as DNA repair, protein metabolism, and inflammatory responses. Compared to traditional lavender extracts and other plant-derived EVs, LELNs offer significant advantages in terms of functional diversity and molecular precision.

While these findings provide a compelling foundation for LELNs as a potential therapeutic, translating this approach into clinical practice requires further development. Delivery strategy is a key consideration, integrating LELNs into biocompatible carriers such as hydrogels, microneedle patches, or lipid-based formulations could enhance their stability and improve dermal penetration in human skin. Such systems would also enable controlled release and targeted action, enhancing therapeutic efficacy[57].

Moreover, achieving scalable and standardized production is essential. While the current isolation protocol is suitable for laboratory studies, future therapeutic use will require reproducible, high-purity LELNs under GMP-compliant conditions. Techniques like ultrafiltration, size-exclusion chromatography, or affinity-based separation could be explored to support large-scale preparation while preserving vesicle integrity[58,59].

Lastly, ensuring the safety and long-term tolerability of LELNs is a necessary step before clinical application. Although plant-derived vesicles are generally considered safe, systematic toxicological evaluations, immunogenicity assessments, and long-term dermal safety studies are needed to confirm their biocompatibility and rule out potential side effects[60].

This study provides strong evidence for the development of LELNs as a novel, multifunctional, and non-invasive therapeutic option for preventing and treating skin photoaging. Continued exploration of their molecular mechanisms, particularly the roles of cpa-miR166e and zma-miR166h-3p, alongside further advancements in delivery strategies, scalable production, and safety evaluation, LELNs hold considerable promise for future applications in skin regeneration, anti-aging therapies, and broader dermatological interventions.

Ethics statement

All experimental procedures and animal care were conducted under the national standard "Requirements for the Environment and Housing Facilities of Laboratory Animals" (GB 14925 – 2010) and adhered to the guidelines established by the National Research Council's Guide for the Care and Use of Laboratory Animals. The study was approved by the Animal Ethics Committee of Qilu University of Technology (Shandong Academy of Sciences) (Approval No. SWS20230711). We confirm that the manuscript of the research report conforms to the ARRIVE guidelines.

Data availability

All available data generated or analyzed during this study are included in this published article, where miRNA sequencing results on lavender samples have been uploaded to the NCBI database, BioSample accession: SAMN46065172.

Received: 16 February 2025; Accepted: 24 June 2025
Published online: 01 July 2025

References

1. Steenvoorden, D. P. & van Henegouwen, G. M. The use of endogenous antioxidants to improve photoprotection. *J. Photochem. Photobiol B.* **41** (1–2), 1–10 (1997).
2. Scharffetter-Kochanek, K. et al. Photoaging of the skin from phenotype to mechanisms. *Exp. Gerontol.* **35** (3), 307–316 (2000).
3. Huang, X. et al. UV-responsive akba@zno nanoparticles potential for polymorphous light eruption protection and therapy. *Mater. Sci. Engineering: C.* **107**, 110254 (2020).
4. Gniadecka, M. et al. Water and protein structure in photoaged and chronically aged skin. *J. Invest. Dermatol.* **111** (6), 1129–1133 (1998).
5. Shin, S. H. et al. Skin aging from mechanisms to interventions: focusing on dermal aging. *Front. Physiol.* **14**, 1664–042X (2023).
6. Gu, Y. et al. Biomarkers, oxidative stress and autophagy in skin aging. *Ageing Res. Rev.* **59** (Electronic), 1872–9649 (2020).
7. Amaro-Ortiz, A., Yan, B. & D'Orazio, J. A. Ultraviolet radiation, aging and the skin: prevention of damage by topical cAMP manipulation. *Molecules* **19** (5), 6202–6219 (2014).
8. Sarasin, A. The molecular pathways of ultraviolet-induced carcinogenesis. *Mutat. Res.* **428** (1–2), 5–10 (1999).
9. Kuilman, T. et al. Oncogene-induced senescence relayed by an interleukin-dependent inflammatory network. *Cell* **133** (6), 1019–1031 (2008).
10. Wang, A. S. & Dreesen, O. Biomarkers of cellular senescence and skin aging. *Front. Genet.* **9** (Print), 1664–8021 (2018).
11. Sha, A. et al. Plant-Derived Exosome-like nanoparticles: A comprehensive overview of their composition, biogenesis, isolation, and biological applications. *Int. J. Mol. Sci.* **25** https://doi.org/10.3390/ijms252212092 (2024).
12. Zhao, B. et al. Exosome-like nanoparticles derived from fruits, vegetables, and herbs: innovative strategies of therapeutic and drug delivery. *Theranostics* **14** (12), 4598–4621 (2024).
13. Wang, X. et al. Plant-Derived Vesicle-like nanoparticles: the Next-Generation drug delivery nanoplatforms. *Pharmaceutics* **16** https://doi.org/10.3390/pharmaceutics16050588 (2024).
14. Gao, C. et al. Plant-derived exosome-like nanoparticles in tissue repair and regeneration. *J. Mater. Chem. B.* **13** (7), 2254–2271 (2025).
15. Liu, R. et al. Plant derived Exosome-Like nanoparticles and their therapeutic applications in glucolipid metabolism diseases. *J. Agric. Food Chem.* **73** (11), 6385–6399 (2025).
16. Kalluri, R. & LeBleu, V. S. The biology, function, and biomedical applications of exosomes. *Science* **367** (6478), eaau6977 (2020).
17. Cao, M. et al. Plant exosome nanovesicles (PENs): green delivery platforms. *Mater. Horiz.* **10** (10), 3879–3894 (2023).
18. Zhang, Z. et al. The emerging role of Plant-Derived Exosomes-Like nanoparticles in immune regulation and periodontitis treatment. *Front. Immunol.* **13**, 896745 (2022).
19. Sarasati, A. et al. Plant-Derived Exosome-like nanoparticles for biomedical applications and regenerative therapy. *Biomedicines* **11** https://doi.org/10.3390/biomedicines11041053 (2023).
20. Lopez de Las Hazas, M. C. et al. Therapeutic potential of plant-derived extracellular vesicles as nanocarriers for exogenous MiRNAs. *Pharmacol. Res.* **198**, 106999 (2023).
21. Marban, E. The secret life of exosomes: what bees can teach Us about Next-Generation therapeutics. *J. Am. Coll. Cardiol.* **71** (2), 193–200 (2018).
22. Perut, F. et al. Strawberry-Derived Exosome-Like nanoparticles prevent oxidative stress in human mesenchymal stromal cells. *Biomolecules* **11** https://doi.org/10.3390/biom11010087 (2021).
23. Şahin, F. et al. Vitro wound healing activity of Wheat-Derived nanovesicles. *Appl. Biochem. Biotechnol.* **188** (2), 381–394 (2019).

24. Savcı, Y. et al. Grapefruit-derived extracellular vesicles as a promising cell-free therapeutic tool for wound healing. *Food Funct.* **12** (11), 5144–5156 (2021).
25. Zu, M. et al. Green' nanotherapeutics from tea leaves for orally targeted prevention and alleviation of colon diseases. *Biomaterials* **279**, 121178 (2021).
26. Kim, D. K. Rhee antioxidative effects of Carrot-Derived nanovesicles in cardiomyoblast and neuroblastoma cells. *Pharmaceutics* **13** https://doi.org/10.3390/pharmaceutics13081203 (2021).
27. Cavanagh, H. M. & Wilkinson, J. M. Biological activities of lavender essential oil. *Phytother Res.* **16** (4), 301–308 (2002).
28. Gezici, S. Promising anticancer activity of lavender (Lavandula angustifolia Mill.) essential oil through induction of both apoptosis and necrosis. *Annals Phytomedicine: Int. J.* **7**, 38–45 (2018).
29. Prashar, A., Locke, I. C. & Evans, C. S. Cytotoxicity of lavender oil and its major components to human skin cells. *Cell. Prolif.* **37** (3), 221–229 (2004).
30. Park, J. & Woo, Y. K. Cho regulation of Anti-Oxidative, Anti-Inflammatory, and Anti-Apoptotic activity of advanced cooling composition (ACC) in UVB-Irradiated human HaCaT keratinocytes. *Int. J. Mol. Sci.* **21** https://doi.org/10.3390/ijms21186527 (2020).
31. Chen, Y. et al. Premna microphylla Turcz pectin protected UVB-induced skin aging in BALB/c-nu mice via Nrf2 pathway. *Int. J. Biol. Macromol.* **215** (Electronic), 1879–0003 (2022).
32. Feng, H. et al. Plant-Derived Exosome-Like nanoparticles: emerging nanosystems for enhanced tissue engineering. *Int. J. Nanomed.* **19** (Electronic), 1178–2013 (2024).
33. Dad, H. A. et al. Plant Exosome-like nanovesicles: emerging therapeutics and drug delivery nanoplatforms. *Mol. Ther.* **29** (1), 13–31 (2021).
34. Stanly, C. et al. Grapefruit-Derived Micro and nanovesicles show distinct metabolome profiles and anticancer activities in the A375 human melanoma cell line. *Cells*. **9**(12), 2722. https://doi.org/10.3390/cells9122722 (2020).
35. Cui, C. et al. Functional Ginger-Derived extracellular Vesicles-Coated ZIF-8 containing TNF-α SiRNA for ulcerative colitis therapy by modulating gut microbiota. *ACS Appl. Mater. Interfaces*. **16** (40), 53460–53473 (2024).
36. Kim, M. Park isolation of Aloe saponaria-Derived extracellular vesicles and investigation of their potential for chronic wound healing. *Pharmaceutics* **14** https://doi.org/10.3390/pharmaceutics14091905 (2022).
37. Bai, C. et al. Research status and challenges of plant-derived exosome-like nanoparticles. *Biomed. Pharmacother.* **174**, 116543 (2024).
38. Calzoni, E. et al. Plant-Derived extracellular vesicles: natural nanocarriers for biotechnological drugs. *Processes* **12** https://doi.org/10.3390/pr12122938 (2024).
39. Nemati, M. et al. Plant-derived extracellular vesicles: a novel nanomedicine approach with advantages and challenges. *Cell. Communication Signal.* **20** (1), 69 (2022).
40. Shao, M. et al. Plant-derived extracellular vesicles -a novel clinical anti-inflammatory drug carrier worthy of investigation. *Biomed. Pharmacother.* **169**, 115904 (2023).
41. Hao, S. et al. Bioactive compounds and biological functions of medicinal plant-derived extracellular vesicles. *Pharmacol. Res.* **200**, 107062 (2024).
42. Lo, K. J. et al. Plant-Derived extracellular vesicles: A new revolutionization of modern healthy diets and biomedical applications. *J. Agric. Food Chem.* **72** (6), 2853–2878 (2024).
43. Chen, X. et al. Plant-derived nanovesicles: Harnessing nature's power for tissue protection and repair. *J. Nanobiotechnol.* **21** (1), 445 (2023).
44. Yadav, A. et al. MicroRNA 166: an evolutionarily conserved stress biomarker in land plants targeting HD-ZIP family. *Physiol. Mol. Biology Plants*. **27** (11), 2471–2485 (2021).
45. Sundaram, K. et al. Plant-Derived Exosomal nanoparticles inhibit pathogenicity of < em > porphyromonas gingivalis. *iScience* **21**, 308–327 (2019).
46. Dobros, N. & Zawada, K. D. Paradowska phytochemical profiling, antioxidant and Anti-Inflammatory activity of plants belonging to the Lavandula genus. *Molecules* **28** https://doi.org/10.3390/molecules28010256 (2023).
47. Byrne, M. E. Shoot meristem function and leaf polarity: the role of class III HD–ZIP genes. *PLoS Genet.* **2** (6), e89 (2006).
48. Hoeijmakers, J. H. DNA damage, aging, and cancer. *N Engl. J. Med.* **361** (15), 1475–1485 (2009).
49. Wouters, M. D. et al. MicroRNAs, the DNA damage response and cancer. *Mutat. Research/Fundamental Mol. Mech. Mutagen.* **717** (1), 54–66 (2011).
50. Zanoaga, O. et al. The role of miR-155 in nutrition: modulating Cancer-Associated inflammation. *Nutrients* **13** https://doi.org/10.3390/nu13072245 (2021).
51. Paladino, S. et al. Nrf2 pathway in Age-Related neurological disorders: insights into MicroRNAs. *Cell. Physiol. Biochem.* **47** (5), 1951–1976 (2018).
52. Qu, L., Wang, F. & Ma, X. The extract from *Portulaca oleracea* L. rehabilitates skin photoaging via adjusting miR-138-5p/Sirt1-mediated inflammation and oxidative stress. *Heliyon*. **9**(11), e21955 (2023).
53. Wlaschek, M. et al. Connective tissue and fibroblast senescence in skin aging. *J. Invest. Dermatol.* **141** (4S), 985–992 (2021).
54. Brenneisen, P., Sies, H., Scharffetter-Kochanek, K., Irradiation, U. B. & Matrix Metalloproteinases. and. Annals of the New York Academy of Sciences, 973(1): pp. 31–43. (2002).
55. Nisar, M. F. et al. Eriodictyol protects skin cells from UVA irradiation-induced photodamage by Inhibition of the MAPK signaling pathway. *J. Photochem. Photobiol., B*. **226**, 112350 (2022).
56. Sharma, P. et al. A comprehensive review of the molecular mechanisms driving skin Photoaging and the recent advances in therapeutic interventions involving natural polyphenols. *South. Afr. J. Bot.* **166**, 466–482 (2024).
57. Lin, S. W., Tsai, J. C. & Shyong, Y. J. Drug delivery of extracellular vesicles: preparation, delivery strategies and applications. *Int. J. Pharm.* **642** (Electronic), 1873–3476 (2023).
58. Paganini, C. et al. Scalable production and isolation of extracellular vesicles: available sources and lessons from current industrial bioprocesses. *Biotechnol. J.* **14** (10), 1800528 (2019).
59. Mu, N. et al. Plant-Derived Exosome-Like nanovesicles: current progress and prospects. *Int. J. Nanomed.* **18** (Electronic), 1178–2013 (2023).
60. Lian, M. Q. et al. Plant-derived extracellular vesicles: recent advancements and current challenges on their use for biomedical applications. *J. Extracell. Vesicles*. **11** (12), 12283 (2022).

Acknowledgements

This work was supported by Technological Small and Medium sized Enterprise Innovation Ability Enhancement Project (2023TSGC0167, 2023TSGC0169), National Key R&D Program Intergovernmental International Science and Technology Innovation Cooperation Project (2023YFE0111900), "Hai You Famous Masters" Industry Leading Talent Support Project (grant number 1362022058), Yantai Development Zone Science and Technology Leading Talents Project (grant number 2020CXRC4, Lin Zhao, and Orlando Borrás - Hidalgo), Key innovation Project of Qilu University of Technology (Shandong Academy of Sciences) (2022JBZ01-06).

Author contributions

Writing—original draft preparation, S.L., S.Z. and X.S.; methodology, S.L.; software, S.L. and L.S.; validation, Q.Y., F.L. and S.Y.; formal analysis, F.L.; investigation, L.Z.; resources, L.Z.; data curation, S.L.; writing—original draft preparation, S.L.; writing—review and editing, S.L.; visualization, S.Y.; supervision, F.L.; funding acquisition, L.Z. All authors have read and agreed to the published version of the manuscript.

Declarations

Competing interests

The authors declare no competing interests.

Conflict of interest

The authors declare that the research was conducted in the absence of any commercial or financial relationships that could be construed as a potential conflict of interest.

Additional information

Supplementary Information The online version contains supplementary material available at https://doi.org/10.1038/s41598-025-08817-2.

Correspondence and requests for materials should be addressed to L.S., S.Y. or L.Z.

Reprints and permissions information is available at www.nature.com/reprints.

Publisher's note Springer Nature remains neutral with regard to jurisdictional claims in published maps and institutional affiliations.